This is a repository copy of *Efficient Radiative Pumping of Polaritons in a Strongly Coupled Microcavity by a Fluorescent Molecular Dye*.

White Rose Research Online URL for this paper:
http://eprints.whiterose.ac.uk/103487/

Version: Accepted Version

Article:

Article type: Full Paper

Title: Efficient Radiative Pumping of Polaritons in a Strongly-Coupled Microcavity by a Fluorescent Molecular Dye

Richard T. Grant[1], Paolo Michetti[2], Andrew Musser[1], Pascal Gregoire[3], Tersilla Virgili[4], Eleonora Vella[3],

Marco Cavazzini[4], Kyriacos Georgiou[1], Francesco Galeotti[4], Caspar Clark[5], Jenny Clark[1], Carlos Silva[3],

David G. Lidzey*[1]

*corresponding author: d.g.lidzey@sheffield.ac.uk

1. Department of Physics and Astronomy, The University of Sheffield, Hicks Building, Hounsfield Road,

Sheffield, S3 7RH, United Kingdom.

2. Institute of Theoretical Physics, Technische Universität Dresden, Zellescher Weg 17, 01062 Dresden,

Germany.

3. Département de Physique, Université de Montréal, C.P. 6128, Succ. centre-ville, Montréal H3C 3J7,

Canada.

4. IFN, ISMAC and ISTM – CNR Milano, Italy

5. Helia Photonics, Livingston, EH54 7EJ, United Kingdom.

Abstract:

We have explored the optical properties of a series of strongly-coupled microcavities containing the fluorescent molecular dye BODIPY-Br (bromine-substituted boron-dipyrromethene) dispersed into a transparent dielectric matrix with each cavity having a different exciton-photon detuning. Using temperature dependent emission, time-resolved spectroscopy, white-light reflectivity and measurements of fluorescence quantum yield, we explore the population of polaritons along the lower polariton branch. We find that both the cavity fluorescence quantum efficiency and the distribution of polariton states along the lower polariton branch is a function of exciton-photon detuning. Importantly, we show that in the most negatively detuned cavities, the emission quantum efficiency approaches that of a control (non-cavity) film. We develop a simple fitting model based upon direct radiative pumping of polariton states along the LPB and use it to obtain an excellent agreement with measured photoluminescence as a function of temperature and exciton-photon detuning, and qualitative agreement with the measured photoluminescence quantum efficiency. The radiative pumping mechanism that we identify indicates that to facilitate the formation of a non-equilibrium polariton condensate in an organic-semiconductor microcavity, it is important to utilize materials having high fluorescent quantum efficiency and fast radiative rates.

A semiconductor-microcavity is an optical structure that can be used to control interactions between light and matter[1]. A typical cavity structure is composed of two mirrors separated by a layer of semiconducting material having a thickness commensurate with the wavelength of light (~100 nm). Such structures confine the local electromagnetic field, and if the energy of the confined photon and excitonic transition are degenerate, interactions can occur in the strong-coupling regime[2–5]. Here exchange of energy between excitons and photons is faster than the photon damping or exciton-photon dephasing, with the eigenstates of the system being cavity polaritons (a coherent superposition between light and matter). Polaritons are observed through an anticrossing

around the resonant energy of the exciton and photon modes in optical reflectivity or photoluminescence (PL) emission measurements[6]. Polaritons are bosonic quasi-particles that exhibit properties of both their excitonic and photonic components, namely the ability undergo scattering through their matter component, to form a coherent polariton condensate[7]. The ability to create and manipulate such condensates offers significant opportunities to create low threshold lasers that operate without the need for a population inversion and devices for quantum-simulations[8–11].

Most studies of strong-coupling have been performed using cavities containing inorganic-based semiconductors such as GaAs[12], CdTe[13], ZnO[14] and GaN[15], either using a bulk semiconductor layer or in more sophisticated quantum well-based structures[6,16]. Recent work has advanced to the point where polariton lasing has now been observed in GaAs[17] and GaN[18] based devices following electrical injection. There is however growing interest in the study of strongly-coupled organic semiconductors, as such materials are generally characterized by high oscillator strengths, large exciton binding energies, and large Rabi splitting energies[19] ($\hbar\Omega_{Rabi}$) (between 50 and 1000 meV) allowing the formation of polaritons to be observed at room temperature[20,21]. A series of organic materials have been explored in strong-coupled microcavities, ranging from porphyrin[4] and phthalocyanine dyes[22], molecular dyes such as anthracene[23], conjugated polymers[24] and oligomers[25], to J-aggregates of cyanine dyes[26]. Recent work has demonstrated polariton lasing from microcavities containing anthracene crystals, conjugated-polymers and a conjugated oligomer[24,27,28]. Polariton electroluminescence has also been evidenced from a number of organic-semiconductor based devices[2,29].

In this paper, we explore emission following non-resonant excitation from a microcavity that contains a fluorescent molecular dye that is doped into an optically transparent matrix. Derivatives of the dye explored (BODIPY-Br) have previously been shown to undergo aggregation to form both H- and J-aggregates[30–32], and our results point to a strong tendency towards excimer formation.

Here, we couple the cavity-photon to a transition associated with the BODIPY-Br monomer species and thereby reach the strong-coupling regime. By varying the exciton-photon detuning, we are able to comprehensively explore the photoluminescence emission from the lower polariton branch as a function of its separation from the so-called 'exciton reservoir'.

By 'exciton reservoir' (ER), we mean the ensemble of excitonic states that remain uncoupled or weakly-coupled to light. This has been shown to play a crucial role in the photo-excitation dynamics of a strongly-coupled micro cavity under non-resonant pumping[33,34], with intra-molecular scattering being the first relaxation step. We emphasise that the properties and the composition of the ER are strongly material (and possibly sample) dependent, as are the different scattering mechanisms that generate the final polariton population and that these are not fully understood. Normally the ER contains uncoupled exciton states derived from molecular states[35], which are also responsible for strong-coupling (in our case, BODIPY monomer excitons) and have a maximum density of states near the bare 'uncoupled' exciton energy. Previous work has demonstrated the scattering to and from such states and the polariton branches is mediated by emission and absorption of molecular vibrations [33,34,36]. However this process can be more varied and complex. Indeed, in materials with intense vibronic replicas, a radiative scattering mechanism mediated by vibronic states has been observed[27] and described theoretically[37,38]. It is also possible, (as we show here) that the ER contains excitonic species that are different in nature than those that undergo strong coupling. This situation has been demonstrated in a strong-coupled microcavity containing a porphyrin dye by Lodden et al[39]. Here a second luminescent low-weight dye was also incorporated into the cavity that emitted light in a spectral range below the main exciton resonance line of the strong-coupled material. Here it was demonstrated that the spontaneous radiative emission of the luminescent dye was able to effectively populate the LPB through a radiative pumping process.

By exploring the dynamics of both cavity and film emission through a variety of techniques including fluorescence quantum yield measurements, angle-resolved PL (CW pump) and time-resolved k-space imaging (pulsed excitation), we conclude that polariton states in this system are most effectively populated via optical pumping by photons emitted from weakly-coupled states within the so-called exciton reservoir. Our work extends the understanding of the mechanisms by which polariton states are populated[40]; a process of key importance in generating a macroscopic occupancy around $k_{//} = 0$, and thus our results are likely to aid the design and construction of low-threshold organic-exciton polariton laser devices.
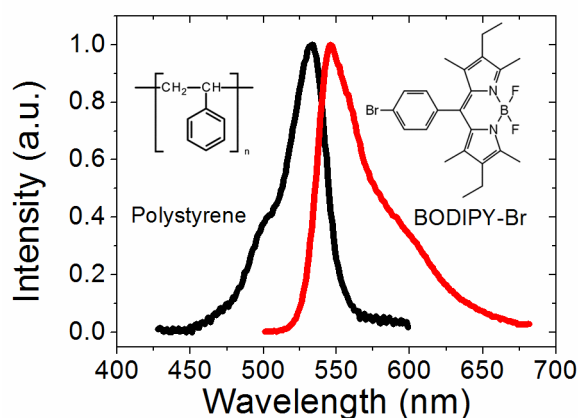
Figure 1. Absorption and PL emission of BODIPY-Br (inset right) doped into a polystyrene (inset left) film at a ratio of 1:100 by mass.

As the active optical material, we have used the molecular dye BODIPY-Br [bromine substituted boron-dipyrromethene] (a variant upon the dipyrromethene family) as shown in **Figure 1**. BODIPY and its variants are noted for their high photoluminescence quantum yield (PLQY), narrow absorption and emission lines, broad solvent compatibility, low triplet-state formation, and high thermal and photochemical stability [41] and have been used as a biological labels[42] and as laser dyes[43]. Importantly, BODIPY-derivatives are known to undergo π−π stacking, with a co-existence between uncoupled monomers, weakly-emissive H-aggregates and J-aggregate-dimers that co-exist

within molecular films at high concentration[30–32]. Such planar π systems can also be susceptible to the formation of stabilized, weakly emissive dimers, or excimers, through excited-state intermolecular relaxation. When doped into a PS matrix at low concentration (1% by mass) BODIPY-Br has a relatively narrow absorption (0-0) transition at 530 nm (2.33 eV) having a FWHM of 15 nm (66 meV), with a (0-1) vibronic replica observed at 500 nm. The PL emission from 1% BODIPY-Br films is characterized by a peak at 542 nm (2.288 eV) having a FWHM of 25 nm (104 meV). The relatively narrow absorption and emission linewidths of BODIPY-Br together with its high PL quantum yield make it an interesting material to study light-matter interactions in strongly-coupled microcavities.
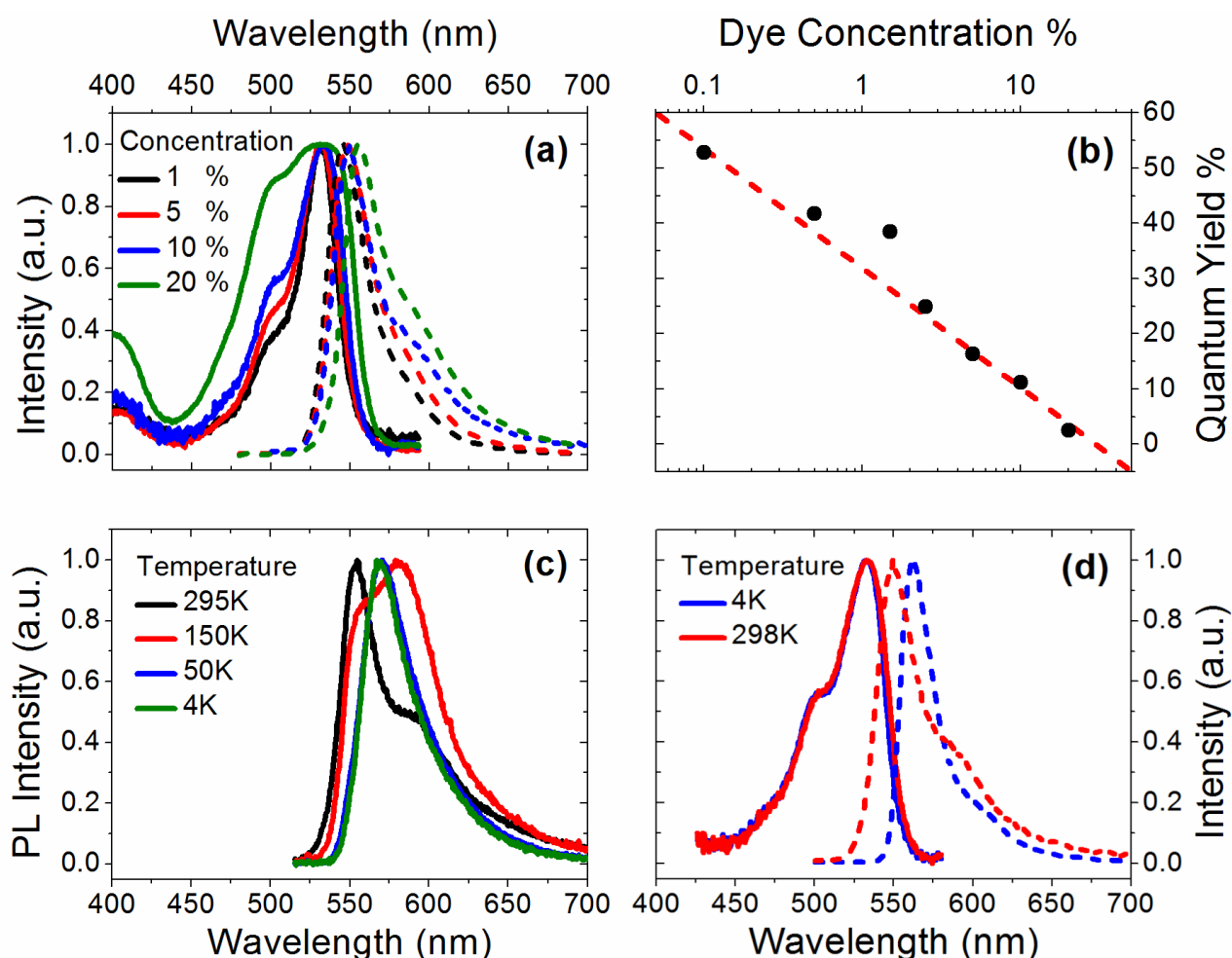

Figure 2. Part (a) shows optical absorption (solid lines) and PL emission (dashed lines) of BODIPY-Br as a percentage concentration in a film of polystyrene. Part (b) shows the PLQY of BODIPY-Br films as a function of concentration. Part (c) depicts PL emission of a film containing

6

BODIPY-Br dispersed in a polystyrene matrix (20% dye by mass) as a function of temperature. In part (d), we plot absorption and PL emission of BODIPY-Br films dispersed in a polystyrene matrix (10% dye by mass) at 4K and 300K.

Results and Discussion:

To process BODIPY-Br into a thin-film that could be deposited into a microcavity, it was dispersed in a polystyrene (PS) matrix. The absorption and emission spectra of a low concentration BODIPY-Br/PS control film (0.1% by mass) is shown in **Figure 1**. At higher relative concentrations of BODIPY-Br in PS, we see a broadening in absorption and PL and a reduction in PLQY as shown in **Figures 2(a)** and **(b)** respectively. Previous work on other BODIPY-derivatives has similarly seen red-shifts and broadening of absorption and have attributed this to the formation of both H- and J-aggregates that co-exist (at lower concentration) with un-aggregated monomers[30]. Critically, we find the PLQY is strongly concentration dependent, ranging from 55% in a film containing 0.1% BODIPY-Br (by mass) to ~5% in films in which the dye concentration is increased to 20%. A significant reduction in PLQY at increased dye concentration has been observed in other BODIPY derivatives, and has been attributed to an increased fraction of molecules forming weakly-emissive or non-fluorescent H-aggregates[30]. On the basis of previous work[30] therefore, we identify the strong absorption at 530 nm with the uncoupled monomeric form of BODIPY-Br, and the broadening at shorter wavelengths with a population of H-aggregates.

However, we find no evidence for the presence of J-aggregates in these films, and instead propose that the red-shifted emission be attributed to excimers. To evidence such states, we have performed temperature-dependent PL spectroscopy (following C.W. excitation at 405 nm) on films having a high concentration (20%) of BODIPY-Br in polystyrene. Typical spectra are shown in **Figure 2(c)** recorded at 298, 150, 50 and 4K. At room temperature, the emission peaks at 555 nm (2.24 eV)

7

[attributed to monomer emission], with a shoulder evident at 588 nm (2.11 eV). As the film is cooled to 4K, we see a significant evolution in the film spectra, with a peak at 570 nm (2.18 eV) emerging from the low-energy shoulder that was observed at room temperature. Previous work has also identified J-aggregates in BODIPY-derivatives around this wavelength[32,44]. However, (as we show using PL excitation spectroscopy in Supplementary Information **Figures S1-3**) there is no corresponding red-shifted absorption for this species, and indeed our measurements at all temperatures demonstrate excitation of the same monomer-like species. Interestingly, we find (using a deconvolution of emission spectra (see **Figures S4-5**)), that as temperature is further reduced, the low-energy emission feature becomes progressively stronger, undergoes a continuous blue-shift, and completely dominates the spectrum by 100K. Through the course of this blue-shift, the spectral shape of the low-energy component remains essentially constant. This behavior is incompatible with H- or J-type aggregation. In light of this and the invariably monomer-like PL excitation spectra, we attribute the low-energy emission in these films to excimers (excited-state molecular dimers). We speculate that the observed blue-shift of the emission reflects a reduction of excited-state conformational freedom as the intermolecular packing becomes denser at low temperature, while the increase in intensity is expected to arise from a reduction in non-radiative decay rates.

A necessary condition to reach the strong-coupling regime in a microcavity is that the Rabi splitting energy is larger than the excitonic absorption linewidth. In organic semiconductors, such transitions are inhomogeneously broadened and can have linewidths of 100s of meV, however by using organic films containing a high concentration of chromophores, very large values of Rabi-splitting can be achieved ($\sim$ 1 eV) as a result of the large oscillator strength (f) of many Frenkel excitons ($\hbar\Omega_{Rabi} \propto \sqrt{f}$). In order to simultaneously reach the strong-coupling regime and to generate efficient luminescence from the BODIPY-Br we have fabricated microcavities containing thin films containing BODIPY-Br at a concentration of 10% by mass (corresponding to a PLQY of

~ 15%). For completeness, we plot the absorption and PL of a film composed of 10% BODIPY-Br in PS at 298K and 4K as shown in **Figure 2(d)**. It can be seen that the absorption of BOIDIPY-Br has negligible temperature dependence. As evidenced in films containing 20% BODIPY-Br, the PL emission appears to be sensitive to temperature. At 298K, we observe strong monomer (0-0) emission at 550 nm (2.250 eV) with a shoulder evident at 580 nm (2.138 eV) (which we assume to originate from a combination of both excimer emission and a relatively broadened 0-1 vibrational transition). At 4K, the main emission peak is red shifted to 563 nm (2.200 eV) and narrowed from 82 meV to 71 meV and comes predominantly from excimers (see analysis in **Figures S3-5**). Compared to room temperature, we find the emission at 4K to be around 20% more intense.
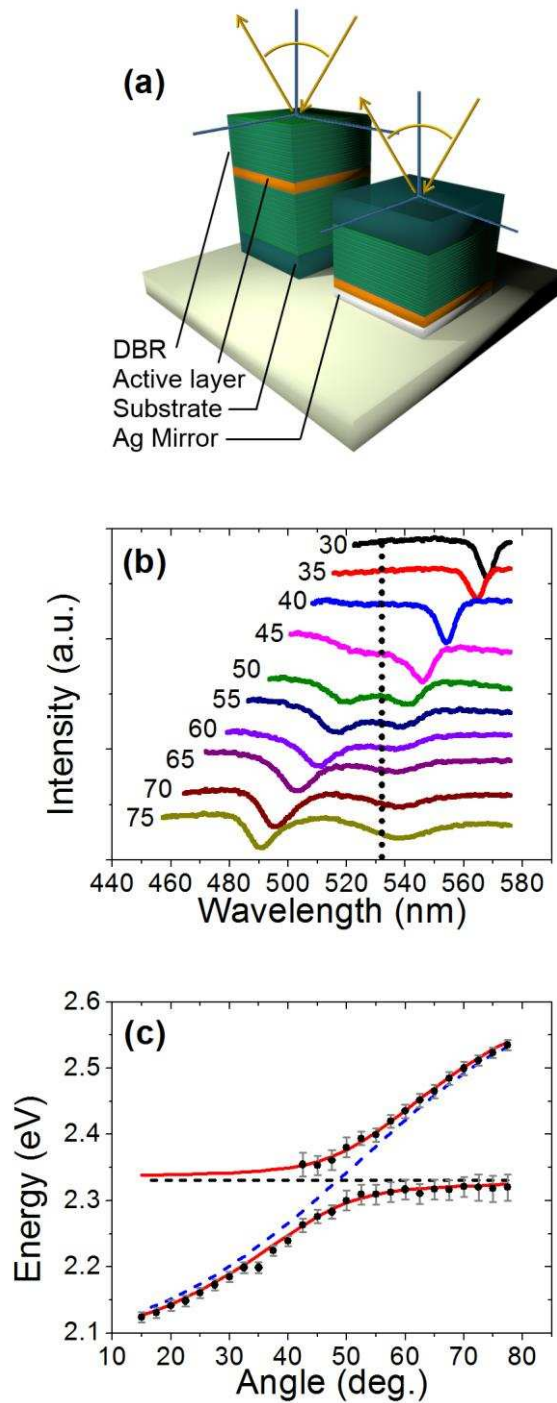
Figure 3. Part (a) shows a schematic of a DBR-DBR (left) and DBR-Metal (right) microcavity structure. Part (b) plots white light reflectivity as a function of external viewing angle of a DBR-Metal microcavity, with part (c) showing a fit of upper and lower polariton branches to measured reflectivity dips shown in part (b).

The microcavities fabricated are shown in **Figure 3(a)** and are designed such that the cavity photon mode undergoes strong-coupling to the main BODIPY-Br absorption transition (corresponding to uncoupled monomers) at ~530 nm. The structures were composed of a 12 pair Distributed Bragg Reflector (DBR) consisting of alternate Nb_2O_5 and SiO_2 layers deposited by ion assisted electron beam and reactive sublimation respectively and were centred at 540 nm. An active BODIPY-Br/PS film was then spin-cast onto the DBR. A second dielectric mirror consisting of 10 mirror pairs was then deposited onto the organic film by the same method. Such microcavities had a Q-factor of ~200. Here all measurements (reflectivity, excitation and emission) were made through the 10 pair DBR as indicated in **Figure 3(a)**. For comparative purposes, a second series of microcavities were also fabricated between a SiO_2 / Si_3N_4 dielectric mirror (deposited by Plasma Enhanced Chemical Vapour Deposition) and a 200 nm silver mirror. Here all measurements (reflectivity, excitation and emission) were made through the DBR. We found that the DBR-Metal cavities had a similar Q-factor of ~150 and thus we feel justified in directly comparing experiments made on either type of structure.

To tune the relative energy-separation of the exciton (E_x) and photon (E_p), the thickness of the BODIPY-Br / PS thin film was tuned between 185 and 290 nm, permitting the exciton-photon detuning (Γ) to be varied between $\Gamma = E_x - E_p = 80$ and 400 meV. To evidence strong coupling in the microcavities, white light reflectance spectroscopy was performed as a function of external viewing angle as shown in **Figure 3(b)** (data shown for a metal-DBR cavity). For comparison, we also plot the angular-dependent reflectivity of a comparable DBR-DBR microcavity in **Figure S6**.

It can be seen that at an angle of $\theta = 30°$, the reflectivity spectrum is characterized by a broad background (originating from the combined reflectivity of the DBR and the metallic mirror) on which a dip at 568 nm (2.183 eV) is superimposed. At increasing viewing angles, this photon-like mode moves closer in energy to the exciton energy (2.33 eV, marked by a dashed line in **Figure**

3(b)) and a second dip emerges at higher energies. At resonance ($\theta = 50°$) the two dips in the spectrum are located either side of the exciton energy. We plot the energy of these features on the dispersion plot shown in **Figure 3(c)** and identify the upper and lower polariton branches (UPB and LPB). It can be seen that as expected, the polariton branches undergo anticrossing around the peak absorption energy of the BODIPY-Br (marked by a horizontal dashed line).

Such behavior can be described using a model of two coupled classical oscillators as described by Equation 1. Here Λ is the interaction potential ($\Lambda = \hbar\Omega_{Rabi} / 2$), $E_p(\theta)$ is the angular dependent photon energy, E_x is the exciton energy and α and β are the Hopfield coefficients corresponding to the relative fraction of photon and exciton mixed into the polariton modes respectively. To account for the dispersion of the cavity photon, we use a standard transfer matrix that includes the average refractive index of the cavity and the energy of the photon-mode at normal incidence (E_p).

$$\begin{pmatrix} E_p(\theta) & \Lambda \\ \Lambda & E_X \end{pmatrix} \begin{pmatrix} \alpha \\ \beta \end{pmatrix} = E \begin{pmatrix} \alpha \\ \beta \end{pmatrix} \tag{1}$$

This equation is solved by diagonalization and then fitted to the measured dispersion curves to extract the Rabi-splitting energy and Hopfield coefficients. For example, from the best fit to the reflectivity dispersion shown in **Figure 3(c)** we determine values of $\hbar\Omega_{Rabi} = 79$ meV, $E_p = 2.11$ eV and $E_x = 2.33$ eV, corresponding to a detuning of 180 meV. The DBR-Metal microcavities studied had values of $\hbar\Omega_{Rabi}$ ranging from 90 to 190 meV and Γ between 80 and 400 meV, while the DBR-DBR microcavities had values of $\hbar\Omega_{Rabi}$ from 65 to 100 meV and Γ between 106 and 345 meV.

To study the emission from DBR-DBR microcavities, they were mounted in a cryostat permitting the role of temperature to be explored. Cavities were excited non-resonantly with k-space imaging used to record the entire polariton dispersion in a single shot. Typical data is shown in **Figure 4**, where we plot the PL emission dispersion for two cavities having different detunings ($\Gamma = 106$ and 290 meV) recorded at 4K and 298K. To exclude the possibility of surface-plasmons contributing to the effects seen here, a series of 'empty' microcavities were fabricated containing a thin film of

12

non-luminescent PS deposited between a DBR and a silver mirror. Reflectivity measurements indicated that such structures were weakly-coupled with the cavity photon mode undergoing a near parabolic dispersion as a function of angle, with no anti-crossing observed. Furthermore we find that following laser excitation at 473nm, no luminescence was detected from such 'empty-cavity' structures. This indicates plasmon-exciton coupling does not contribute to strong coupling and that any plasmon-emission generated is below the noise floor of our detector (see **Figure S7**).
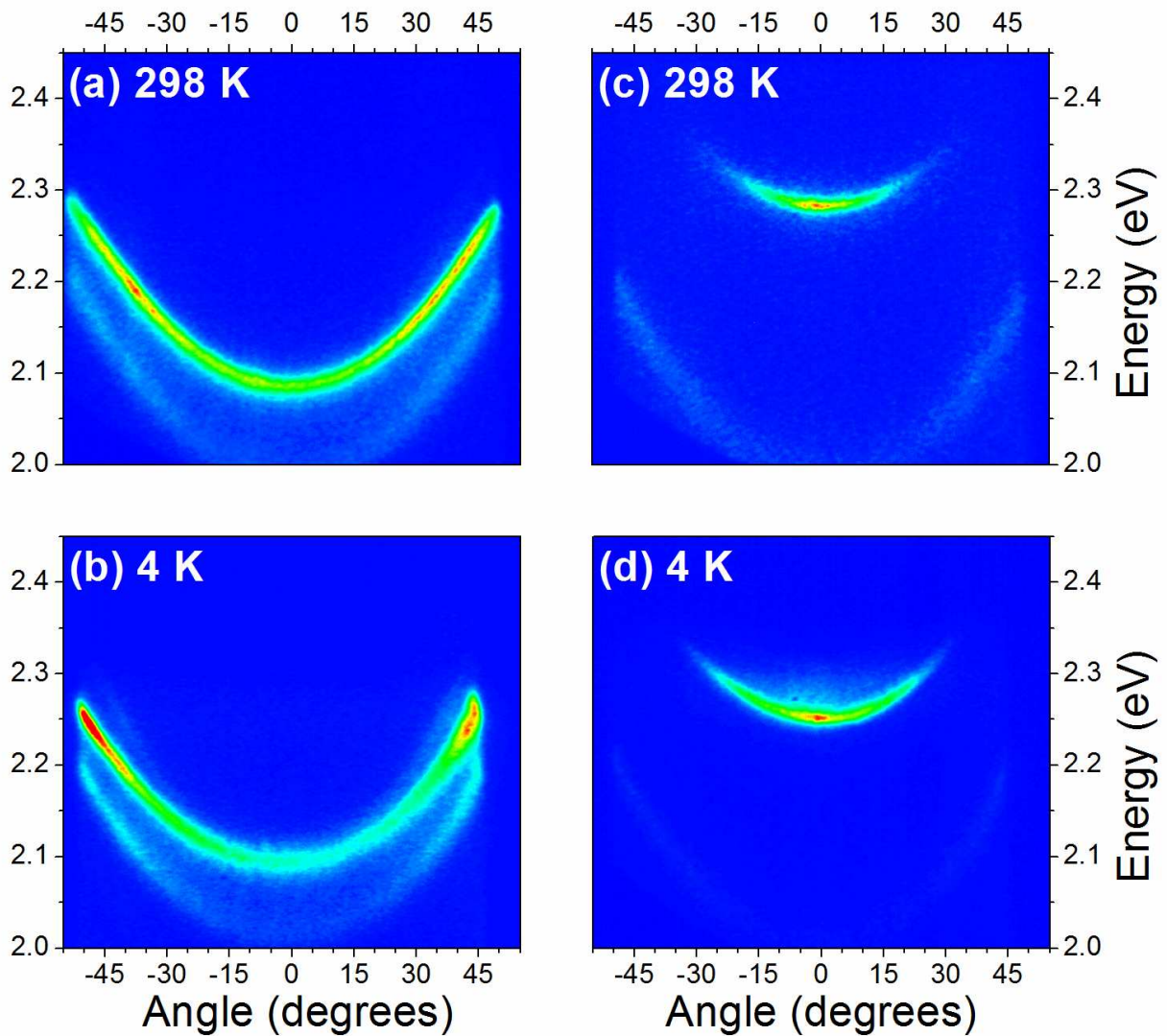

Figure 4. Fluorescence emission from microcavities having a detuning of 290 meV (parts (a) and (b)), and 106 meV (parts (c) and (d)) at cryogenic (4K) and room temperature (298K). Here emission was generated using with a pulsed pump laser and recorded using a k-space imaging

setup. All four dispersions plots have been individually normalized to clearly depict overall population distribution.

Typical emission from two cavities having different detunings (Γ = 106 and 290 meV) recorded at 4K and 298K is shown in **Figure 4**. We find that for both cavities, no PL emission is detected from the UPB, with the intense luminescence detected in all cases corresponding to the energy of the LPB as detected in reflectivity measurements. Note, a weak emission feature with a near parabolic dispersion located at an energy ~100 meV below that of the LPB is detected. This emission corresponds to light escaping the cavity through the first minima of the DBR stopband which also has a strong angular dependence.

In **Figure 4**, it can be seen that strong PL emission is observed from the LPB (a finding that is also observed in cavities that also incorporate metallic mirrors). In particular, it can be seen that at 298 K, emission from the cavity having the smaller detuning (Fig 4(c)) is strongly concentrated towards the bottom of the LPB (i.e. around θ = 0º). In the cavity having the much larger detuning (Fig 4(a)), the emission pattern is qualitatively different, with emission apparently distributed evenly along the LPB. When the temperature is reduced to 4K, we find that emission from the cavity having the smaller detuning (Fig 4(d)) is still concentrated towards the bottom of the LPB, however a significant change is observed in the cavity having the larger detuning (Fig 4(b)), with emission now concentrated around points on the LPB (θ > 30º), corresponding to states close in energy to the exciton reservoir. Our measurements therefore indicate that thermalization of the excitation is incomplete and that relaxation to large detunings is ineffective. The mechanism of population of the polariton branches appears to be both energy- and temperature-dependent, being more effective in the spectral region near the exciton reservoir. This is consistent with the observed change in the photoluminescence emission as can be seen in **Figure 2(d)**.

To further explore emission from the cavity structures, the fluorescence decay lifetime from cavities was recorded as a function of time following a pump pulse, with measurements performed

at 4K and 298K. It was found that the PL emission decay dynamics of both BODIPY-Br control films and the microcavities can be described by the sum of two exponentials (see supplementary figures **S8-9**), having fast and slow time constants of ≤ 300 ps and $2 - 5$ ns with lifetime and amplitudes dependent on detection wavelength and temperature (see data summary in **Table S1**). Previous work has similarly evidenced a multi-exponential decay from BODIPY-Br films, and has interpreted this on the basis of dipole-dipole energy transfer between monomeric and aggregated forms of the molecule.[30] Here, we associate the longer-lifetime decay components observed with excimer states that have reduced radiative rates[45], and believe that the combination of fast and slow decay kinetics to be consistent with dipole-dipole energy transfer between isolated monomers and sites where excimers can form. Significantly however, we find that the decay lifetimes recorded from the cavities and the control films are in most cases similar (within a factor of two).
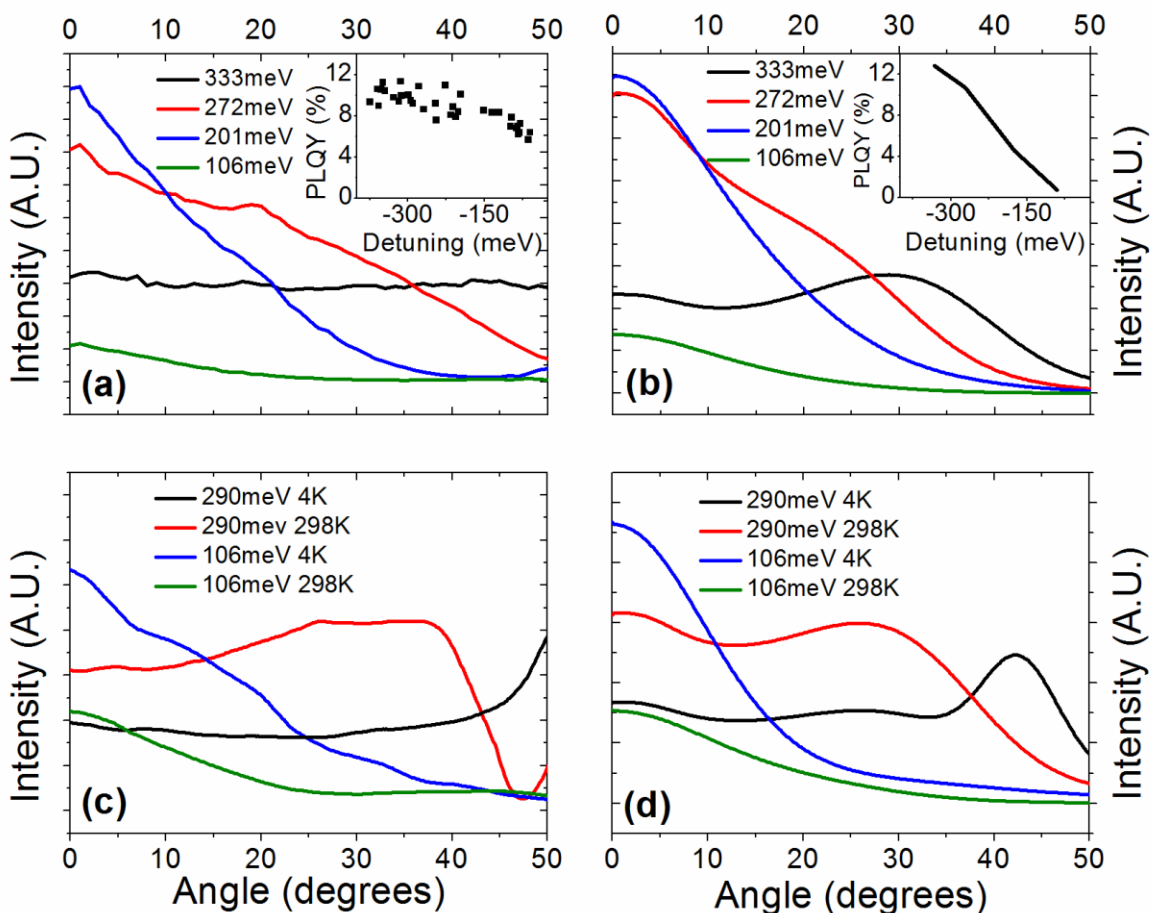

15

Figure 5. Part (a) plots the measured PL intensity at 298K as a function of angle for four DBR-DBR microcavities having detunings of Γ = 333, 272, 201 and 106 meV. Part (b) plots the simulated PL intensity as a function of angle for the same four detunings. In part (c) we plot the PL emission intensity measured at 298K and 4K for cavities having a detuning of Γ = 290 and 106 meV. Part (d) plots the calculated PL intensity for the cavity emission shown in part (c). Inset: (left) is the measured PLQY of a series of DBR-Metal microcavities having detunings ranging from Γ= 80 to 400 meV. Inset (right) simulated PLQY as a function of detuning.

The similarity between cavity and control film decay rates (at least in a low pump-density regime) has been observed in a number of systems[46–48], and indicates that polariton states along the LPB are populated relatively slowly from the exciton reservoir, and do not significantly change the overall emission dynamics of the BODIPY-Br. To gain a more quantitative understanding of the population of polariton states, the PLQY from the microcavities was measured using an integrating sphere using previously reported methods as given by Green et al.[49] This measurement was performed for a large number of metal-DBR cavities having a range of detunings, and is shown in **Figure 5(a)**.

Despite some scatter in the data, it is clear that microcavities possessing larger negative exciton-photon detuning generally emit luminescence with greater efficiency than do cavities having a smaller detuning; specifically cavities having the greatest (smallest) detuning have a PLQY of 11% (6%), with the efficiency of emission of the control film being 15%. The similarity between the PLQY of the control film of BODIPY-Br and that of the most negatively detuned cavities suggests the following polariton-population scenario: following optical excitation of an exciton, rapid relaxation inside the BODIPY-Br molecular film populates a reservoir of uncoupled states positioned at lower energies than the main absorption transition. These weakly coupled excitons are able to decay by emission of a photon that radiatively-pumps a strongly-coupled polariton state. The

16

similarity in the PLQY of emission from cavities having a large detuning and that of the control film confirms that this process can be quite efficient.

To confirm this hypothesis, we have developed a phenomenological model describing the mechanisms of polariton population from the exciton reservoir that lead to polariton emission under continuous non-resonant excitation. Photoexcitation relaxation is taken into account using a series of rate equations describing the particle exchange between the exciton reservoir (ER) states and the UPB and LPB. The polariton branches are divided into annular regions, labelled by the modulus of the wave vector k, of energy $E_{k,U}$ and $E_{k,L}$ for UPB and LPB, containing N_k states. The division of the polariton density of states in homogeneously populated annular regions is supported by the isotropy of the microcavity emission. The inhomogeneously broadened ER is described in the model by a single state having an effective FWHM of 30 meV. We assume that non-resonant pumping directly populates the ER. It is also assumed that the ER is composed of monomeric dye molecules that are each described as a two-level-system that undergoes strong-coupling. In this idealised picture, a polariton state is described by equation (2) as a superposition of a photon mode $|\vec{k}\rangle_{ph}$ and an exciton component delocalized over the whole film, with equal weight distributed between N dye monomers ($|j\rangle$):

$$|\vec{k}\rangle = \alpha(k)|\vec{k}\rangle_{ph} + \beta(k)\sum_j^N \frac{e^{i\vec{k}\vec{r}_j}}{\sqrt{N}}|j\rangle \qquad (2)$$

Following the model developed for J-aggregate films and J-aggregate microcavities[50,33,34], we initially tried to describe the exciton-polariton scattering process mediated by the emission/absorption of a molecular vibration, localised on each monomer dye molecule or in the host matrix. Here we explored a scattering process summarised by equation (3), where W_0 and p are fitting parameters, with $n(E)$ being the Bose-Einstein distribution.

$$W_{k\leftarrow X} = W_0|E_k - E_X|^p \frac{|\beta(k)|^2}{N}[1 + n(E_k - E_X)] \qquad (3)$$

17

We find that this approach can explain the relative suppression of UPB PL (but not its complete absence) via a rapid depletion of the UPB states through the effective scattering of polaritons back to the ER accompanied with the emission of a vibrational quanta. However to explain the variation of the LPB emission intensity observed in the experiments, we needed to invoke unrealistic changes in the parameters W_0 and p as a function of the detuning of the microcavity. A second process is therefore needed. Considering the fluorescent nature of the dye monomer, we postulate a mechanism whereby excitons in the ER radiatively pump polariton states as described by equation (4), where E_1 and σ are fitting parameters that describe the energy and linewidth of the weakly-coupled exciton states involved in the pump-process.

$$W_{k \leftarrow x} = W_1 e^{\frac{-(E_k - E_1)^2}{2\sigma^2}} |\alpha(k)|^2 \tag{4}$$

This model assumes that ER states possess at least two electronic transitions; a high oscillator strength 0-0 transition being responsible for strong-coupling together with a population of weakly coupled states that are able to undergo spontaneous emission and 'pump' states along the LPB. A similar process was first invoked to explain the optical population of polaritons in crystalline anthracene; microcavities in which the 0-0 transition was strongly-coupled and emission from the weakly-coupled 0-1 transition pumped states at the bottom of the LPB[37,38]. We note that in other work, microcavities have been constructed that contain both strongly- and weakly-coupled components, with a polariton population being generated via weakly-coupled radiative emission[51]. In the present case we pragmatically adopt a simple Gaussian emission profile to describe the shape of the weakly-coupled emission pumping the LPB. We will later discuss the issue of the exact nature of such weakly-coupled emission in the present system, which as we show below seems temperature activated. Surprisingly, we find that a single pump-reservoir described by parameters E_1 = 2.086 eV (593 nm) and σ = 58 meV (16 nm) results in a quite reasonable fit describing the

polariton PL emission as a function of emission angle at all microcavity detuning values explored. This can be seen in **Figure 5**, where we plot the photoluminescence emission intensity following non-resonant CW excitation recorded at 298K as a function of angle for 4 different cavities having a detuning of $\Gamma = 333, 272, 201$ and 106 meV in part (a), with the modelled emission intensity shown in part (b).

Interestingly the best fit to the data suggests that this radiative relaxation mechanism is the dominant process that populates the LPB, with exciton to polariton scattering following the emission/absorption of a vibrational quanta being a rather ineffective channel. We can also fix the absolute value of the scattering rate W_1, by means of the PLQY. We determine a PLQY from a control film of BODIPY-Br (10% in PS by mass) of the order of 15%, and using a PL decay time of the order of 3 ns, a non-radiative exciton quenching time of $\tau_x = 3.5$ ns is determined. This then suggests that ER excitations have a non-radiative depletion rate of $1/\tau_x$. By using a value of W_1 (≈ 3 x 10^3 s^{-1} in equation (4)), we can provide a quite reasonable description of the PLQY of the microcavities as a function of their detuning value as shown in **Figure 5**. By integrating the radiative pumping process along the LPB ($K = \sum_{LPB} W_{k \leftarrow X}$), a physically meaningful life-time ($\tau = K^{-1}$) for each cavity can be calculated, with times determined between 20 ns for the microcavity having the most significant negative detuning, to 1 ms for cavities having much smaller detunings. Our model allows us to understand the dependence of PLQY as a function of cavity detuning; cavities having a greater detuning have a larger fraction of more photon-like states that exist at larger viewing angles. These states are more efficiently pumped by the reservoir, and their subsequent radiation increases the relative photon yield from the lower polariton branch. It is clear however that for microcavities that possess small detunings, the present model fails to completely reproduce the measured PLQY, although it provides a reasonable qualitative description of the measured PL emission along the LPB.

To further explore the validity of the model, we have used it to simulate the PL emission from cavities having a detuning of Γ = 290 and 106 meV at 4K and 298K. Here, experimental data is plotted in **Figure 5(c)**, with the results of the calculation plotted in 5(d). Again it can be seen that good qualitative agreement is obtained between measured and modelled results. Importantly however, it is necessary to modify the radiative term at 4K to include a second pump emission peak at 2.18 eV (567 nm), with the peak at 2.086 eV (593 nm) being relatively diminished in amplitude but remaining present. The parameters used in the radiative pumping terms are summarised in Table 1.

Table 1. Parameters used to fit the angular-dependent cavity population. E denotes the energy of each emission peak included, A the amplitude, and D the width of each peak.

Temp.	E_1	E_2	A_1	A_2	D_1	D_2
K	meV	meV	-	-	meV	meV
300	2086	-	1	-	82	-
4	2086	2180	0.5	1	82	30

We now discuss the nature of the weakly-coupled states that pump the LPB polaritons. We interpret our results on the basis of the thin-film emission spectra, in which we observed photoluminescence from two distinct BODIPY-Br species: monomers and excimers. As shown in Table 1, a single pump term at E_1 = 2.086 eV (593 nm) appears to be sufficient to describe the polariton emission at 298K. As can be seen in **Figure 2(c) and Figure S5**, this wavelength seems close in energy to the excimer emission at 2.06 eV (602 nm). At 4K, the additional pump term at E_2 = 2.18 eV (567nm) that is necessary to describe the cavity population appears to coincide with intense, blue-shifted excimer emission observed in the neat films at 2.202 eV (563 nm) (see **Figure 2(d)**). In the microcavity, the excimer states are weak-coupled and can therefore radiatively pump the polariton states at all temperatures. We can thus identify emission from excimers with both the

E_1 and E_2 pump terms: the former is sufficient to describe the high-temperature excimer spectrum, while at low temperatures the emission is better described as a combination of the two.

This picture is able to explain the temperature-dependant behaviour of the control film PL and identify the presence and relative importance of E_1 and E_2 pumping terms in the model at low- and room-temperature. At room temperature, a significant fraction of the exciton population is quenched in the weakly emissive excimer state, which corresponds to the E_1 pumping term, with some contribution from the emission of the degenerate 0-1 vibronic monomer transition also being possible. Note that the migration of 0-0 exciton population into various states at lower energy that are unable to undergo vibrationally-assisted scattering to or from the polariton branches is consistent with the absence of UPB luminescence. At low temperature, energy relaxation in the film follows the same pathway as before, but the nature of the weakly coupled state partially changes, enabling even more efficient optical pumping of states along the LPB (the E_2 term) from enhanced excimer luminescence. However weaker pumping from the E_1 term is still observed. We note that the relative reduction in the amplitude (A_1) of the lower-energy (E_1) pump-term required to describe cavity emission at 4K is consistent with the lineshape of the excimer emission observed at that temperature (See **Figure 2(c)**). Our model thus suggests the apparent redistribution of polariton population that occurs along the LPB as a function of temperature observed in microcavities having a large energetic detuning appears to originate from changes in the energetic excitation distribution within the ER, rather than some type of polariton thermalisation process.

It is instructive to compare our work with other recent work on strong-coupled organic microcavities. Ballarini et al[28] fabricated a series of strongly coupled microcavities using a squaraine dye having a low PLQY of < 0.01%, and observed large enhancements in PLQY from the cavity (up to an order of magnitude for resonant pumping); a result in direct contrast with the small reduction in PLQY observed here. The difference between such findings can be understood on the basis of the relative magnitudes of radiative decay of uncoupled reservoir excitons and the exciton

21

to polariton scattering rate. Here, our model indicates that direct radiative pumping of polaritons by weak-coupled excimer decay is a much more efficient process than phonon-assisted exciton-polariton scattering process, and thus the net yield of photons emitted from the cavity is largely unchanged in the strong-coupling regime. In contrast, in cavities containing materials having a low radiative rate (or reduced PLQY)[28], the exciton to polariton scattering rate can be comparable to radiative decay and thus the additional generation of additional highly-radiative polaritons can increase the overall photon yield substantially.

Conclusions:

In conclusion, we have demonstrated strong coupling in a series of microcavities containing the fluorescent molecular dye BODIPY-Br and have investigated the change in polariton distribution along the lower polariton branch as a function of detuning and temperature. It is found that as the exciton-photon detuning is reduced, the polariton population is increasingly concentrated around the bottom of the lower polariton branch. Measurements of photoluminescence quantum efficiency indicates that the overall yield of photons from the cavity is similar to that of a non-cavity control film, and that the photoluminescence decay lifetime of cavity and control films are quite similar. To understand such observations, a fitting model is used that describes the population of polaritons following weakly-coupled radiative decay of reservoir excitons. Surprisingly, it is found that this radiative pumping process provides an adequate description of the cavity emission over a large range of detunings at room temperature and at 4K, with the model indicating that phonon-mediated exciton-to-polariton scattering does not contribute substantially to the polariton population mechanism. Indeed, it appears to be similar to cavities containing crystalline anthracene[27], though in such systems no change in the energy of the radiative pumping term was observed as a function of temperature. Here, π-π interactions between BODIPY-Br molecules is likely to give rise to co-existing spectral signatures of well-isolated monomers and excimers. Using a phenomenological fitting model, we suggest the population along the lower polariton branch to be the result of the

optically pumping due to emission from the weakly-coupled vibronic 0-1 monomer transition and a stabilized, temperature-dependent excimer state.

The relatively high photoluminescence emission quantum yield of BODIPY-Br, together with the high efficiency by which lower polariton branch states are populated make the cavities studied here a strong candidate in which to observe polariton condensation and lasing. The importance of the radiative pumping mechanism identified here suggests that polariton condensation thresholds in organic-semiconductor microcavities can most likely be reduced by using molecular materials having a high photoluminescence quantum efficiency and a high radiative rate.

Methods:

<u>Fluorescence quantum yield</u>

PLQY from the microcavities was measured (integrated over energy and external viewing angle) following excitation at 500 nm (2.48 eV) using light from a SC400 Fianium supercontinuum laser filtered by a SPEX 270M monochromator. Light emitted by the microcavities was captured by placing them inside an integrating sphere. PLQY was calculated by comparing the relative intensities of the incident laser with and without the sample present. This difference was then compared to the total amount of light emitted by the cavity.

<u>White light reflectivity:</u>

Microcavity samples were mounted on a rotation stage that consisted of two independent rails that pivoted around the sample. White-light reflectivity was measured by focusing light from a Tungsten-Halogen lamp through optics mounted on one of the rails onto the cavity surface, with the reflected beam collected by optics mounted on the second rail that was then imaged into a fiber-optic cable coupled to an Ocean Optics spectrometer. DBR-DBR microcavities were measured through the top (less-reflective) ten pair DBR. Reflectivity measurements on DBR-Metal microcavities were however performed with white-light incident on the DBR through the quartz substrate.

<u>CW pump photoluminescence:</u>

Samples were mounted on a rotation stage as described above, with light from a laser diode (3000μW 405 nm) incident on the sample at close to normal incidence (i.e. non-resonant excitation). Emission was collected by optics mounted on one rail of the rotation stage, and focused into a fibre-optical cable connected to an Andor Shamrock CCD spectrometer. DBR-DBR microcavities were excited through the top (less-reflective) ten pair DBR, with emission also collected through this DBR. DBR-Metal microcavities were excited through the quartz substrate/DBR, with emission also collected through the DBR.

24

<u>Time resolved k-space imaging:</u>

To explore the distribution of polaritons following non-resonant excitation, 200 fs pulses at 343 nm from a Yb:KGW laser operating at a repetition rate of 600 kHz and a 3rd harmonic generator were used to excite polariton photoluminescence with emission dispersed over k-space imaged onto an Acton SP-2300i spectrometer coupled to a Lavision Picostar ICCD (nominal time resolution of 200 ps). Samples were mounted in a cryostat permitting the role of temperature to be explored by using liquid helium to reach temperatures of 4K.

<u>BODIPY-Br / PS control-film absorption and emission:</u>

BODIPY-Br / PS control-films were mounted on the cold-finger of a closed-cycle Oxford Instruments cryostat that was cooled to 4K. Samples were pumped non-resonantly using a 473 nm diode laser. Emission was collected at normal incidence and focused into a fibre-optical cable connected to an Ocean Optics CCD spectrometer.
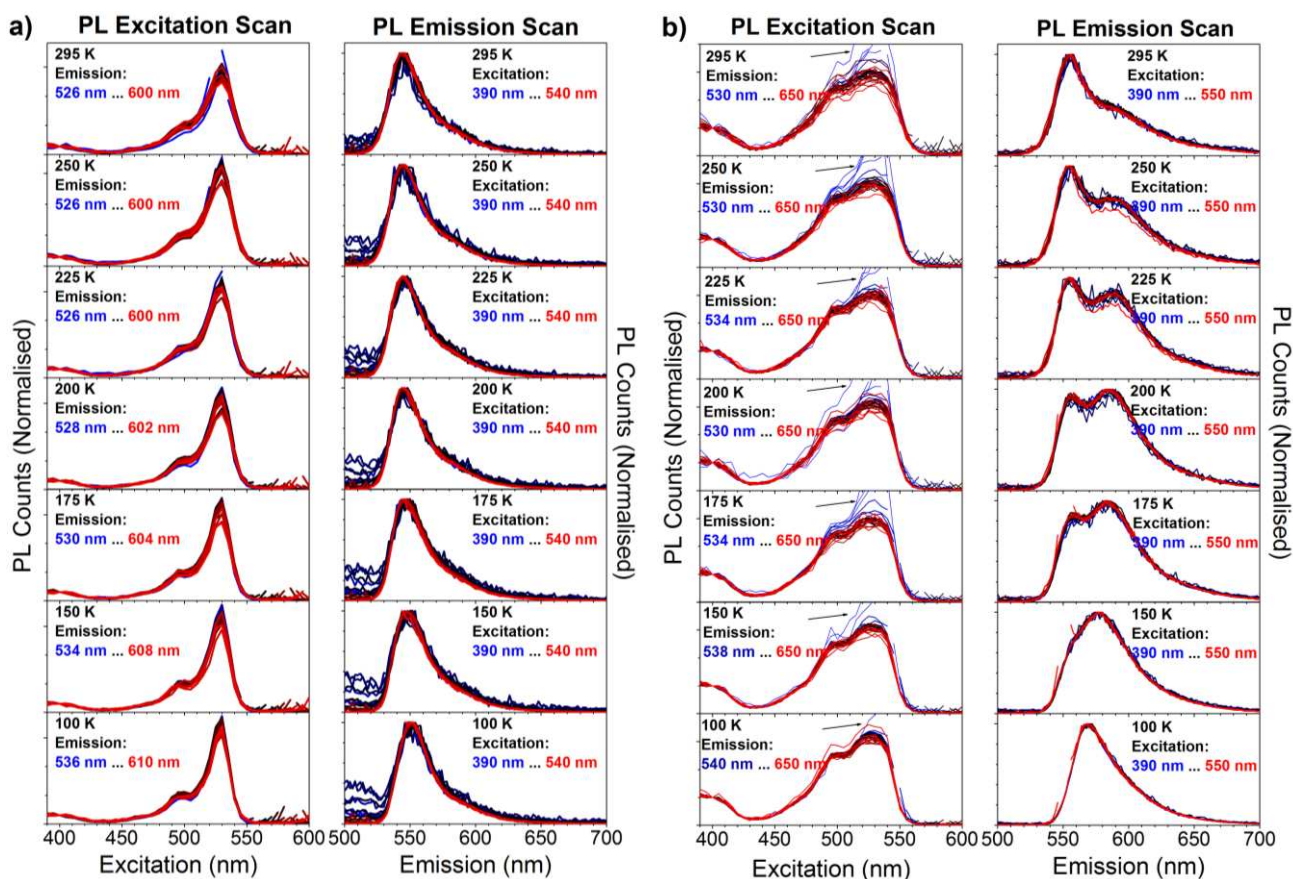
Supplementary Information:
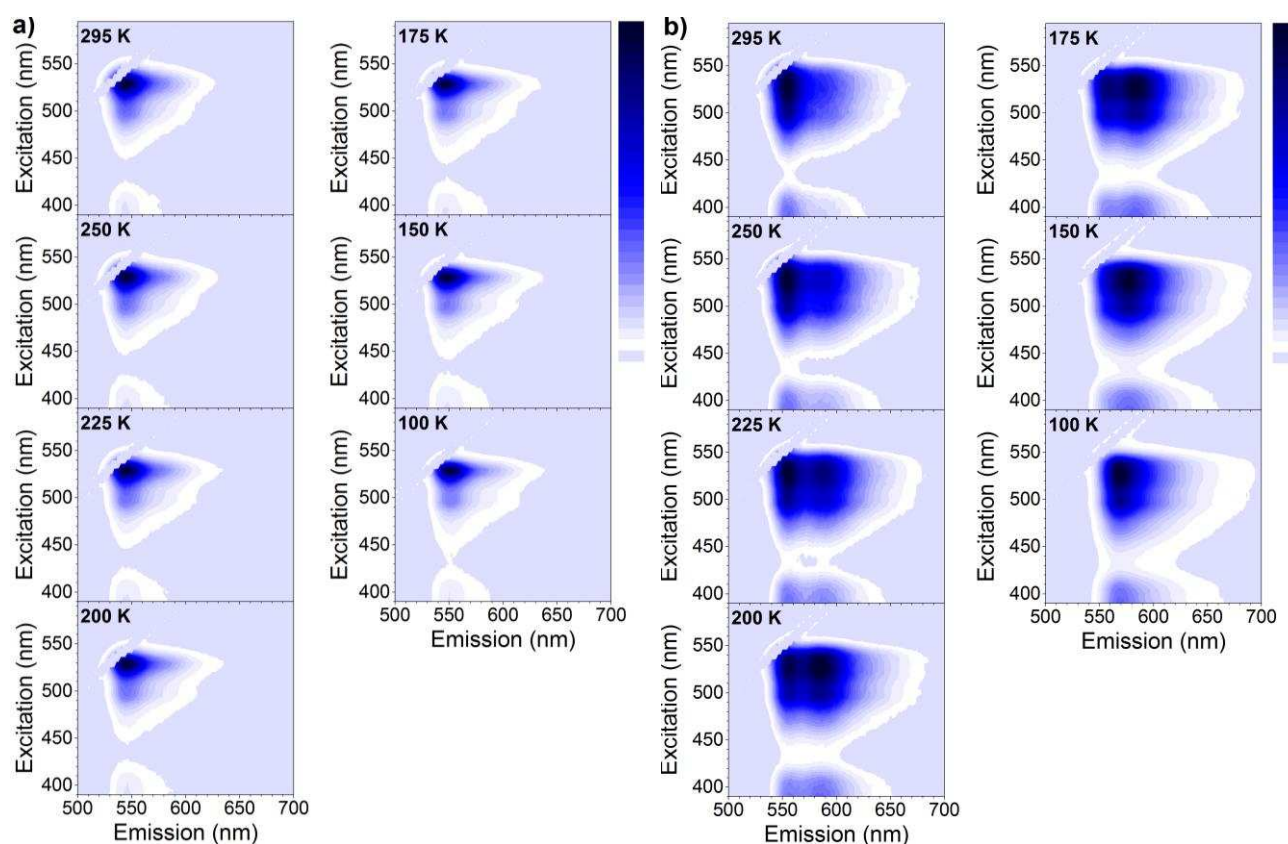
Supplementary Figure S1. PLE maps of BODIPY-Br in polystyrene, taken over a temperature range spanning all important spectral changes. (a) Dilute 1% film. Only a slight red-shift (~6 nm) is observed at low temperatures, with no change in spectral shape. (b) In the concentrated 20% film, we observe a growth of the red-shifted emission feature as the temperature is reduced. temperature. This feature undergoes a progressive blue-shift as temperature is reduced, and at low temperature it merges with and then dominates the short-wavelength monomeric emission peak around 550nm. (compare peak positions at 150 K and 100 K). However, no corresponding changes in the apparent absorption of the film can be detected (vertical axis). For both films, the temperature series was measured in the order 295-250-200-150-100-175-225-295 K to ensure no permanent changes to the film were induced. Monochromators were set to 1 nm for excitation and emission. Excitation was

scanned in 5 nm steps, while emission was scanned in 2 nm steps. Maps are all normalized to the same colour scale.


Supplementary Figure S2. Normalized spectral cuts of the PLE maps above along each emission wavelength (left column) or excitation wavelength (right column), for (a) 1% films, and (b) 20% films reveal no sub-gap states or aggregates, at any temperature. In the dilute film, the only spectral changes are a slight narrowing and redshift at low temperature: at this concentration the molecule behaves as a well-isolated chromophore. (b) In concentrated films, PL excitation reveals an invariant absorption lineshape at every temperature. Similarly, at any one fixed temperature, we do not observe changes in the PL spectrum as a function of excitation wavelength. In all cases, the same initial population (resembling monomeric BODIPY-Br) is photo-excited. However, the overall red-shift is twice that observed in dilute films (~12 nm) and is accompanied by new long-

wavelength PL features and a significant thermally-activated increase in relative PL efficiency (see Figure S4 below). These effects cannot be explained from intramolecular properties and must arise from intermolecular interactions. Unlike in previous studies of BODIPY aggregates, there is no evidence in excitation spectra of distinct 'sub-gap' aggregate absorption. These effects are thus most consistent with an intermolecular quenching pathway active only in the excited state, namely excimer formation. PL excitation spectra are shown in 4 nm steps of emission wavelength. PL emission spectra are shown in 10 nm steps of excitation wavelength. Black arrows denote points where the excitation scatter distorts the lineshape.
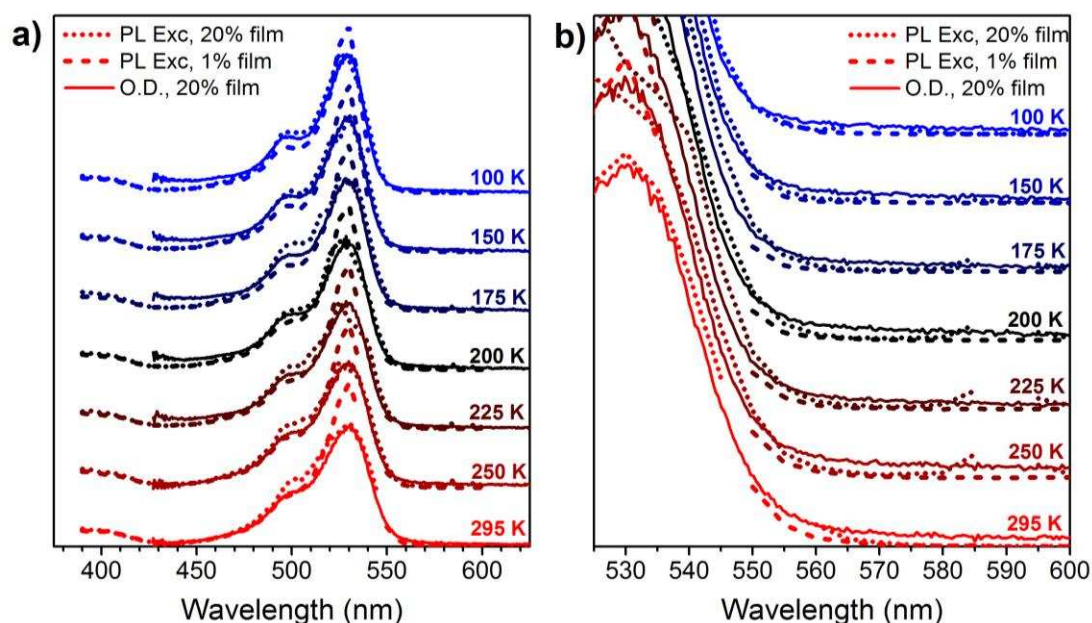

Supplementary Figure S3. (a) Temperature-dependent PL excitation spectra for 20% (dotted) and 1% (dashed) BODIPY-Br films, taken at the emission maximum from Figure S1, and converted into optical density scale for comparison with the film absorption (solid). All spectra show the same lineshape at each temperature, apart from slight broadening in the 20% film spectra. (b) At the band edge, there is no evidence of additional sub-gap absorbing species in the concentrated film (dotted, solid). In particular, at 100 K where the red-shifted emission is most pronounced, the low- and high-

concentration PLE spectra overlap completely. The red-emitting species is only accessed through excitation of the monomer, as in an excimer. Spectra are scaled to have comparable magnitude.
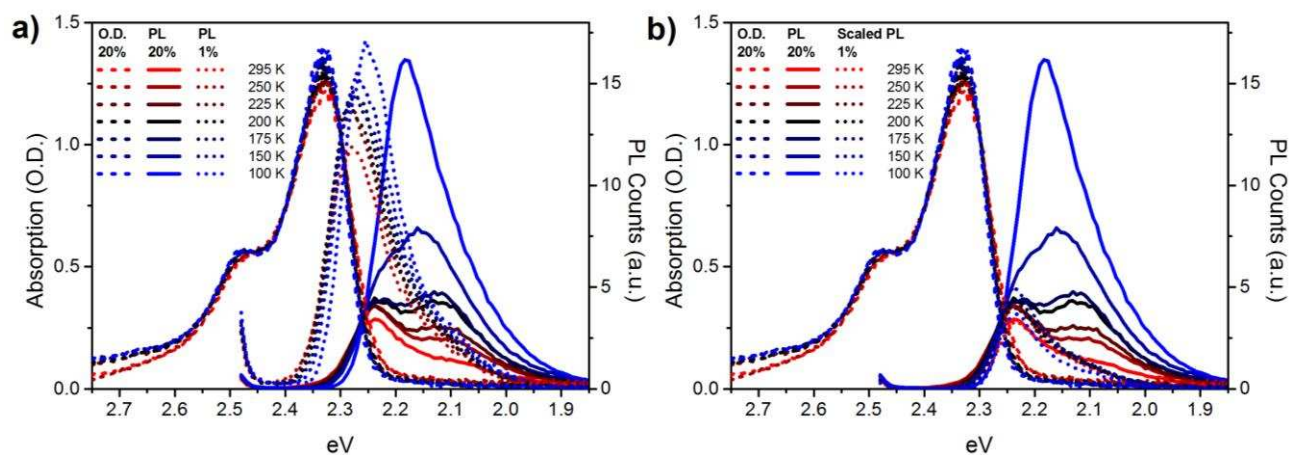

Supplementary Figure S4. (a) Temperature-dependent absorption (dashed) and PL (solid) of 20% BODIPY-Br/PS films, and PL of 1% BODIPY-Br/PS films (dotted). PL spectra were collected with excitation at 495 nm (2.51 eV), and the growth in intensity (by a factor of ~3.8x from 295 K to 100 K at high concentration, versus ~1.3x at low concentration) reflects an increased PL quantum yield as the temperature is reduced. As temperature is reduced, the 20% BODIPY-Br absorption spectrum sharpens and slightly blue-shifts at the band edge, and additional absorption can be detected in the high-energy region previously attributed to non-emissive H-aggregates. It is evident from the significant overlap of absorption and 1% film emission, and the high optical density of the concentrated films, that the large shift of PL spectral edge between 1% and 20% films can be largely attributed to self-absorption. (b) To distinguish the effects of aggregate- and monomer-type emission, we have scaled the PL of the 1% film (dotted) by the absorption spectrum of the concentrated film at each wavelength. This gives an approximation of self-absorption effects. The spectra were then scaled by a variable factor (between 1 and 2) to match the intensity of concentrated-film PL (solid) at the high-energy edge. The agreement of peak positions and PL edge

is excellent at all temperatures. Note the size of the monomer contribution signified by the scaled 1% spectra does not vary significantly through the temperature series.
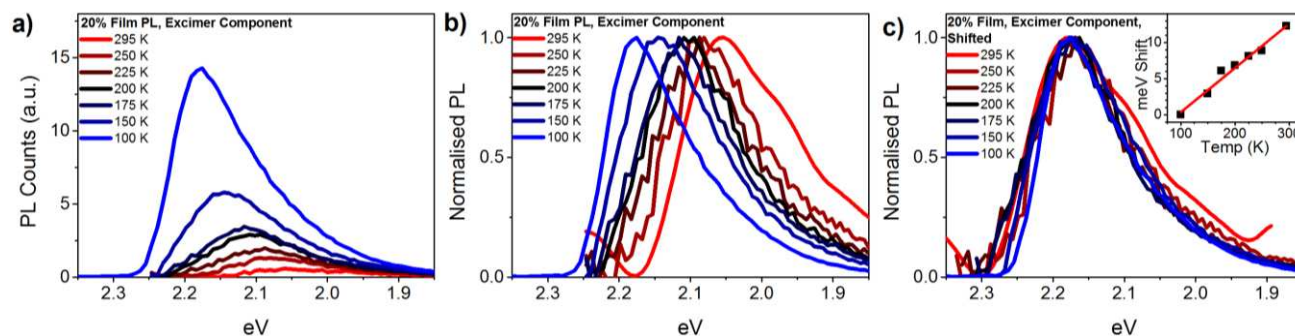

Supplementary Figure S5. Isolated excimer emission. (a) Following subtraction of the self-absorption-corrected monomer (i.e. 1% film) contribution (Figure S4), we are left with the PL spectrum of the red-shifted species. The emission of this species progressively blue-shifts and increases in intensity as the temperature decreases. Such an increase in intensity is consistent with a reduction in the rates of non-radiative decay. (b) Upon normalisation, the gradual shift of the entire spectrum with temperature is strong evidence that no new species appear. Rather, the low-energy species responsible for radiative pumping at room temperature gradually increases in energy (and PL yield) as the temperature is decreased. Thus the 'same' population is responsible for radiative pumping at both temperature extremes. (c) Manually shifting the red-shifted spectrum at each temperature to overlap with that at 100 K, we find no variation in the spectral shape within the noise of the measurement, except for at most a slight narrowing at low temperature. The degree of spectral shift appears to vary linearly with temperature (inset). This behaviour would not be expected of any type of aggregate (any change in J- or H-type character would result in a change in relative vibronic peak ratios). Given the stability of the spectral shape over the temperature range, the lack of vibronic structure and the absence of any signatures in PL excitation or ground-state absorption of a distinct red-emitting species, we assign this emission to an excimer.
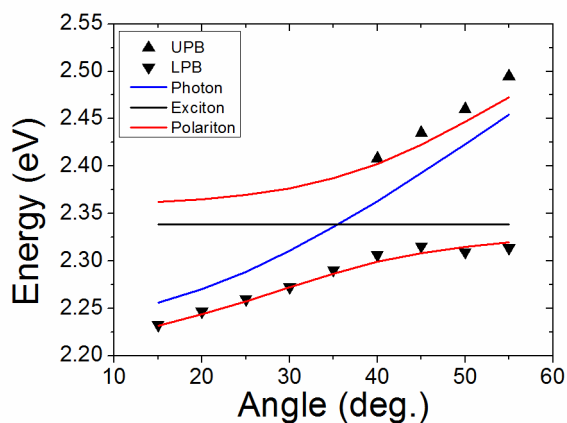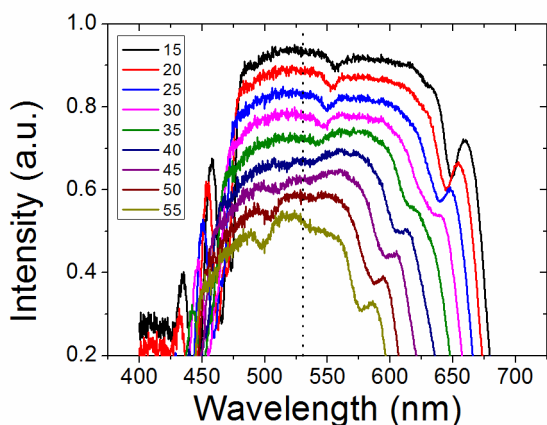
**Supplementary Figure S6.** Reflectivity dispersion of a strongly coupled DBR-DBR microcavity
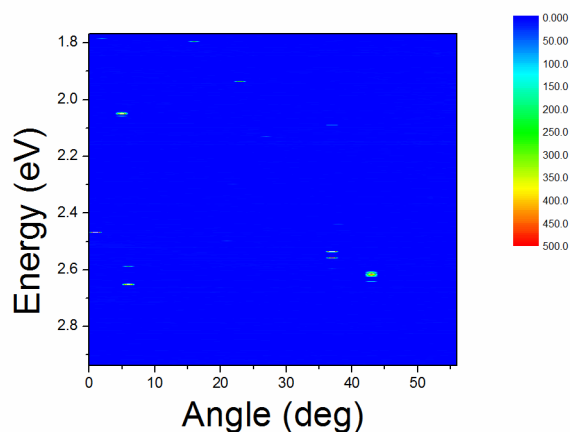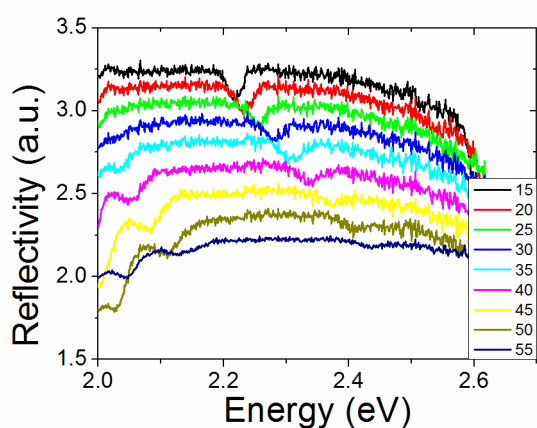
Supplementary Figure S7. Reflectivity (left) and PL (or lack thereof, right) data from a microcavity containing a blank spacer layer of polystyrene to exclude the possibility of plasmon contribution to observed PL. Scattered points observed in PL data most probably correspond to cosmic rays or detector noise.
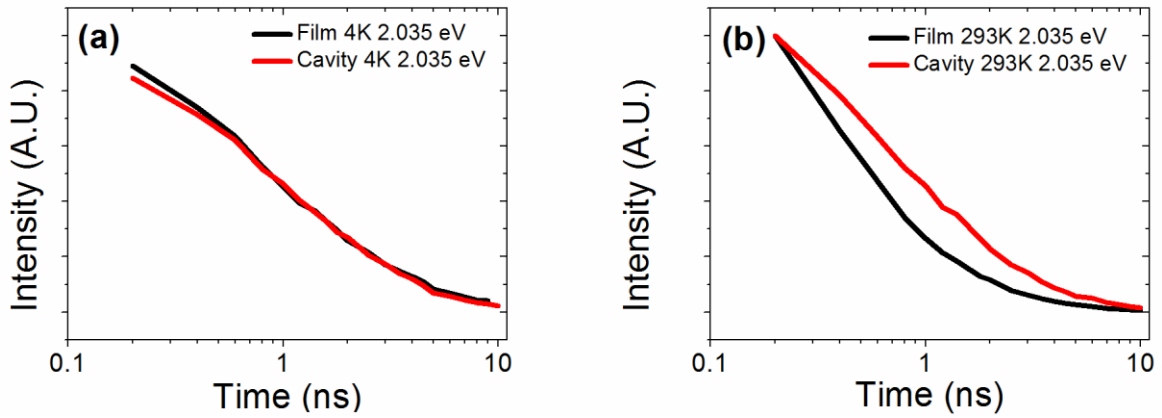
Supplementary Figure S8. PL decay time comparison for control films and a microcavity with detuning of 290 meV at (a) 4K and (b) 298K
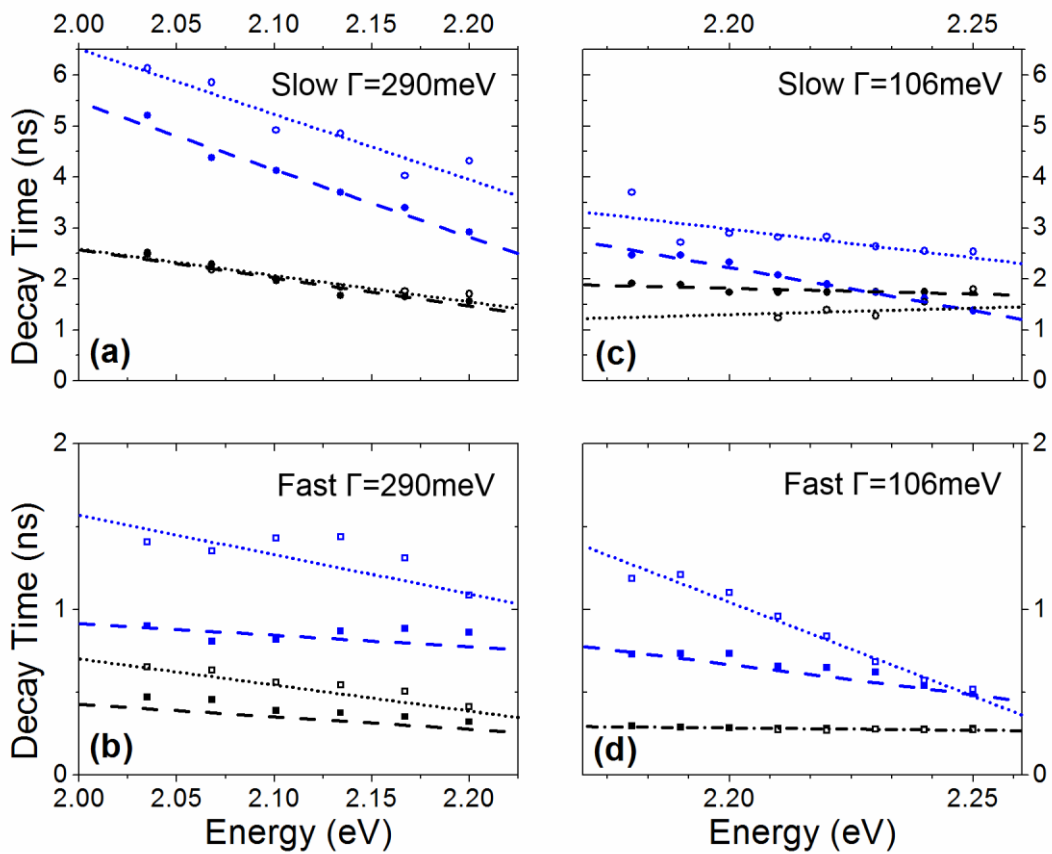
Supplementary Figure S9. PL decay time constants of control films (solid markers) and microcavities (open markers) at 298K (black) and 4K (blue) for detunings of Γ = 290 meV (left,

parts (a) and (b)) and $\Gamma = 106$ meV (right, parts (c) and (d)) as a function of detection energy. The top panels (parts (a) and (c)) summarise the slow decay components whilst the bottom panels (parts (b) and (d)) plot the fast decay components which coincide with the temporal resolution of the detector (~250 ps).

Supplementary Table1. PL decay time constants for Supplementary Figure 1.

	τ_1 4K	τ_1 298K	τ_2 4K	τ_2 298K	A/B 4K	A/B 298K
Units	(ns)	(ns)	(ns)	(ns)	(ratio)	(ratio)
Cavity-small detuning	0.57-1.2	0.27	2.5-2.9	1.6-2	180-340	165-250
Film-small detuning range	0.5-0.75	0.27-0.29	1.3-2.4	1.7-1.9	5-15	270-290
Cavity large detuning	1.1-1.4	0.41-0.65	4.3-6.1	1.7-2.2	15-25	7-90
Film-large detuning range	0.8-0.9	0.32-0.47	3-5.2	1-1.7	7-9	35-70

Decay constants for different points along the LPB are compared to the decay times for the corresponding energies of a control film of the same concentration (10% by mass), at 4K and at 298K. The components correspond to the formula: $I = Ae^{-\tau_1/t} + Be^{-\tau_2/t} + C$ where I represents measured PL intensity, τ_1 and τ_2 represent decay constants for the fast and slow components, and A and B represent their relative amplitudes.

REFERENCES

[1] K. J. Vahala, *Nature* **2003**, *424*, 839.

[2] J. Tischler, M. S. Bradley, V. Bulović, J. Song, A. Nurmikko, *Phys. Rev. Lett.* **2005**, *95*, 036401.

[3] M. S. Skolnick, T. A. Fisher, D. M. Whittaker, *Semicond. Sci. Technol.* **1998**, *13*, 645.

[4] D. G. Lidzey, D. D. C. Bradley, M. S. Skolnick, T. Virgili, S. Walker, D. Whittaker, *Nature* **1998**, *395*, 53.

[5] R. F. Oulton, N. Takada, J. Koe, P. N. Stavrinou, D. D. C. Bradley, *Semicond. Sci. Technol.* **2003**, *18*, S419.

[6] M. Ilegems, U. Oesterle, *Phys. Rev. Lett.* **1994**, *73*, 2043.

[7] D. Snoke, *Nat. Nanotechnol.* **2013**, *8*, 393.

[8] P. Tsotsis, P. S. Eldridge, T. Gao, S. I. Tsintzos, Z. Hatzopoulos, P. G. Savvidis, *New J. Phys.* **2012**, *14*, 023060.

[9] A. Imamoglu, R. J. Ram, S. Pau, Y. Yamamoto, *Phys. Rev. A* **1996**, *53*, 4250.

[10] H. Deng, G. Weihs, D. Snoke, J. Bloch, Y. Yamamoto, *Proc. Natl. Acad. Sci. U. S. A.* **2003**, *100*, 15318.

[11] A. Kavokin, G. Malpuech, F. P. Laussy, *Phys. Lett. A* **2003**, *306*, 187.

[12] D. Bajoni, E. Semenova, A. Lemaître, S. Bouchoule, E. Wertz, P. Senellart, J. Bloch, *Phys. Rev. B* **2008**, *77*, 113303.

[13] M. Richard, J. Kasprzak, R. André, L. S. Dang, R. Romestain, *J. Phys. Condens. Matter* **2004**, *16*, S3683.

[14] L. K. van Vugt, S. Rühle, P. Ravindran, H. C. Gerritsen, L. Kuipers, D. Vanmaekelbergh, *Phys. Rev. Lett.* **2006**, *97*, 147401.

[15] G. Christmann, R. Butté, E. Feltin, A. Mouti, P. Stadelmann, A. Castiglia, J.-F. Carlin, N. Grandjean, *Phys. Rev. B* **2008**, *77*, 085310.

[16] S. Christopoulos, G. von Högersthal, a. Grundy, P. Lagoudakis, a. Kavokin, J. Baumberg, G. Christmann, R. Butté, E. Feltin, J.-F. Carlin, N. Grandjean, *Phys. Rev. Lett.* **2007**, *98*, 126405.

[17] C. Schneider, A. Rahimi-Iman, N. Y. Kim, J. Fischer, I. G. Savenko, M. Amthor, M. Lermer, A. Wolf, L. Worschech, V. D. Kulakovskii, I. a Shelykh, M. Kamp, S. Reitzenstein, A. Forchel, Y. Yamamoto, S. Höfling, *Nature* **2013**, *497*, 348.

[18] P. Bhattacharya, T. Frost, S. Deshpande, M. Z. Baten, A. Hazari, A. Das, *Phys. Rev. Lett.* **2014**, *112*, 236802.

[19] S. Kéna-Cohen, S. a. Maier, D. D. C. Bradley, *Adv. Opt. Mater.* **2013**, *1*, 827.

[20] T.-C. Lu, J.-R. Chen, S.-C. Lin, S.-W. Huang, S.-C. Wang, Y. Yamamoto, *Nano Lett.* **2011**, *11*, 2791.

[21] D. G. Lidzey, D. D. C. Bradley, T. Virgili, A. Armitage, M. S. Skolnick, S. Walker, *Phys. Rev. Lett.* **1999**, *82*, 3316.

[22] D. G. Lidzey, T. Virgili, D. Bradley, M. Skolnick, S. Walker, D. Whittaker, *Opt. Mater. (Amst).* **1999**, *12*, 243.

[23] M. Litinskaya, P. Reineker, V. M. Agranovich, *Phys. Status Solidi* **2004**, *201*, 646.

[24] J. D. Plumhof, T. Stöferle, L. Mai, U. Scherf, R. F. Mahrt, *Nat. Mater.* **2013**, *13*, 1.

[25] K. S. Daskalakis, S. A. Maier, R. Murray, S. Kena-Cohen, *Nat. Mater.* **2014**, *13*, 271.

[26] D. M. Coles, N. Somaschi, P. Michetti, C. Clark, P. G. Lagoudakis, P. G. Savvidis, D. G. Lidzey, *Nat. Mater.* **2014**, *13*, DOI 10.1038/NMAT3950.

[27] S. Kena-Cohen, S. R. Forrest, *Nat. Photonics* **2010**, *08*, 1.

[28] D. Ballarini, M. De Giorgi, S. Gambino, G. Lerario, M. Mazzeo, A. Genco, G. Accorsi, C. Giansante, S. Colella, S. D'Agostino, P. Cazzato, D. Sanvitto, G. Gigli, *Adv. Opt. Mater.* **2014**, *2*, 1076.

[29] N. Christogiannis, N. Somaschi, P. Michetti, D. M. Coles, P. G. Savvidis, P. G. Lagoudakis, D. G. Lidzey, *Adv. Opt. Mater.* **2013**, *1*, 503.

[30] T. T. Vu, M. Dvorko, E. Y. Schmidt, P. Retailleau, B. A. Tro, R. B. Pansu, G. Clavier, R. Me, *J. Phys. Chem.* **2013**, *117*, 5373.

[31] S. Choi, J. Bouffard, Y. Kim, *Chem. Sci.* **2014**, *5*, 751.

[32] I. Mikhalyov, N. Gretskaya, F. Bergström, L. B.-A. Johansson, *Phys. Chem. Chem. Phys.* **2002**, *4*, 5663.

[33] P. Michetti, G. C. La Rocca, *Phys. Rev. B* **2008**, *77*, 195301.

[34] P. Michetti, G. C. La Rocca, *Phys. Rev. B* **2009**, *79*, 035325.

[35] P. Michetti, G. C. La Rocca, *Phys. Rev. B* **2005**, *71*, 115320.

[36] M. Litinskaya, P. Reineker, V. M. Agranovich, *J. Lumin.* **2004**, *110*, 364.

[37] L. Mazza, L. Fontanesi, G. C. La Rocca, *Phys. Rev. B* **2009**, *80*, 235314.

[38] L. Mazza, S. Kéna-Cohen, P. Michetti, G. C. La Rocca, *Phys. Rev. B* **2013**, *88*, 075321.

[39] G. H. Lodden, R. J. Holmes, *Phys. Rev. B - Condens. Matter Mater. Phys.* **2010**, *82*, 1.

[40] P. Michetti, L. Mazza, G. C. La Rocca, in *Org. Nanophotonics* (Ed.: Y.S. Zhao), Springer, Berlin, Heidelberg, **2015**, pp. 39–68.

[41] G. Ulrich, R. Ziessel, A. Harriman, *Angew. Chem. Int. Ed. Engl.* **2008**, *47*, 1184.

[42] F. J. Monsma, A. C. Barton, H. C. Kang, D. L. Brassard, R. P. Haugland, D. R. Sibley, *J. Neurochem.* **1989**, *52*, 1641.

[43] M. Shah, K. Thangaraj, M.-L. Soong, L. T. Wolford, J. H. Boyer, *Heteroat. Chem.* **1990**, *1*, 389.

[44] S. Kim, J. Bouffard, Y. Kim, *Chem. - A Eur. J.* **2015**, *21*, 17459.

[45] S. A. Jenekhe, J. A. Osaheni, *Science ,80,* **1994**, *265*.

[46] T. Schwartz, J. A. Hutchison, J. Léonard, C. Genet, S. Haacke, T. W. Ebbesen, *ChemPhysChem* **2013**, *14*, 125.

[47] F. Tassone, C. Piermarocchi, V. Savona, A. Quattropani, P. Schwendimann, *Phys. Rev. B* **1996**, *53*, 7642.

[48] D. G. Lidzey, A. Fox, M. Rahn, M. Skolnick, V. Agranovich, S. Walker, *Phys. Rev. B* **2002**, *65*, 195312.

[49] A. P. Green, A. R. Buckley, *Rev. Sci. Instrum.* **2012**, *83*, 073108.

[50] D. J. Heijs, V. A. Malyshev, J. Knoester, *Phys. Rev. Lett.* **2005**, *95*, 177402.

[51] G. M. Akselrod, E. R. Young, M. S. Bradley, V. Bulovi, *Opt. Express* **2013**, *21*, 3691.